Eur. Phys. J. D **8**, 23–28 (2000)

THE EUROPEAN PHYSICAL JOURNAL D

EDP Sciences

Impact broadening and shift rates for the $6p^2\ ^3P_{J'} \rightarrow 7s\ ^3P^o_J$ transitions of lead induced by collisions with argon and helium

J. Franzke[1,2], H.D. Wizemann[1], K. Niemax[2], and C. Vadla[3,a]

[1] Institute of Physics, Universität Hohenheim, Garbenstrasse 30, 70599 Stuttgart, Germany
[2] Institute of Spectrochemistry and Applied Spectroscopy (ISAS), Bunsen-Kirchhoff-Strasse 11, 44139 Dortmund, Germany
[3] Institute of Physics, Bijenicka 46, 10000 Zagreb, Croatia

Received 27 April 1999

Abstract. The collisional broadening and shift rate coefficients of the 283.39 nm ($6p^2\ ^3P_0 \rightarrow 7s\ ^3P^o_1$), 364.06 nm ($6p^2\ ^3P_1 \rightarrow 7s\ ^3P^o_1$), 368.45 nm ($6p^2\ ^3P_1 \rightarrow 7s\ ^3P^o_0$) and 405.90 nm ($6p^2\ ^3P_2 \rightarrow 7s\ ^3P^o_1$) Pb lines by He and Ar have been measured by fitting the experimental absorption line shapes to theoretical Voigt profiles. The absorption measurements were performed in a resistively heated, Pb loaded oven with an integrated dc noble gas discharge to produce also Pb atoms in the $6p^2\ ^3P_1$ and $6p^2\ ^3P_2$ metastable states. The diffusion of the metastable atoms out of the discharge zone into the neutral noble-gas atmosphere enabled the line-shape and shift measurement of the lines involving the metastable states without the influence of the discharge plasma.

PACS. 32.70.Jz Line shapes, widths, and shifts

1 Introduction

There is still a considerable theoretical interest in the pressure broadening and shift of spectral lines since the data provide information on fundamental long-range interactions between the optical atom and its collision partners. On the other hand, the line shape parameters are needed in different fields of application. For example, line broadening data are of interest for plasma diagnostics, in astrophysics, or analytical spectroscopy. Comprehensive reviews on pressure broadening and shift of spectral lines are published by Ch'en and Takeo [1] and Allard and Kielkopf [2]. A rather complete bibliography of theoretical and experimental papers published between July 1978 and March 1992 is available from NIST [3].

Unfortunately, there is an unsatisfactory status concerning the foreign gas broadening and shift data of Pb lines. As one can take from [3], there are a few investigations on Pb lines broadened by neutral atoms. Among those, there are no papers related to the noble gas broadening and shift of the lines reported here. In the more recent literature, there is only one paper dealing with the noble gas broadening and shift of the resonance 283.39 nm line [4], whereas there are, to our knowledge, no experimental or theoretical data available for the 364.09 nm, 368.45 nm and 405.90 nm lines.

In a current project on the development of spectrochemical techniques for the analysis of heavy elements in low-pressure noble gas discharges we are interested in the excitation, collision and diffusion processes of the analyzed atoms, as well as in their effective lifetimes in metastable states. In order to model the behaviour of the heavy elements in the discharge collisional broadening data are required.

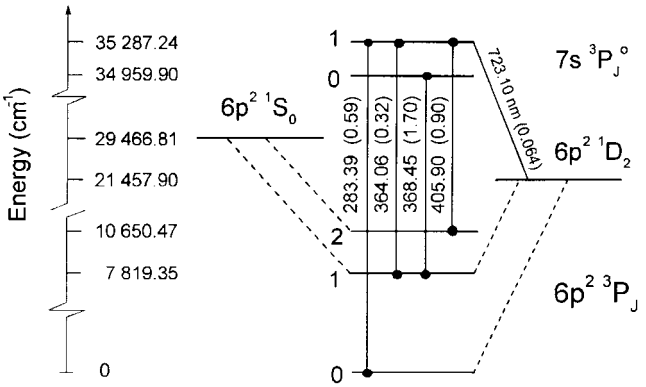

Fig. 1. Partial term diagram of Pb. The wavelengths are given in nanometers. The numbers in brackets are the corresponding transition probabilities in 10^8 s^{-1}. The dashed lines indicate dipole forbidden transitions.

The present work reports on noble gas impact broadening and shift of the fine-structure lines belonging to the $6p^2\ ^3P_{J'} \rightarrow 7s\ ^3P^o_J$ multiplet transition of Pb. The $6p^2\ ^3P_{J'}$ substates are the lowest-lying states of Pb (see Fig. 1), where the $6p^2\ ^3P_0$ is the ground state, while the $6p^2\ ^3P_1$ and $6p^2\ ^3P_2$ are metastable states.

[a] e-mail: vadla@ifs.hr

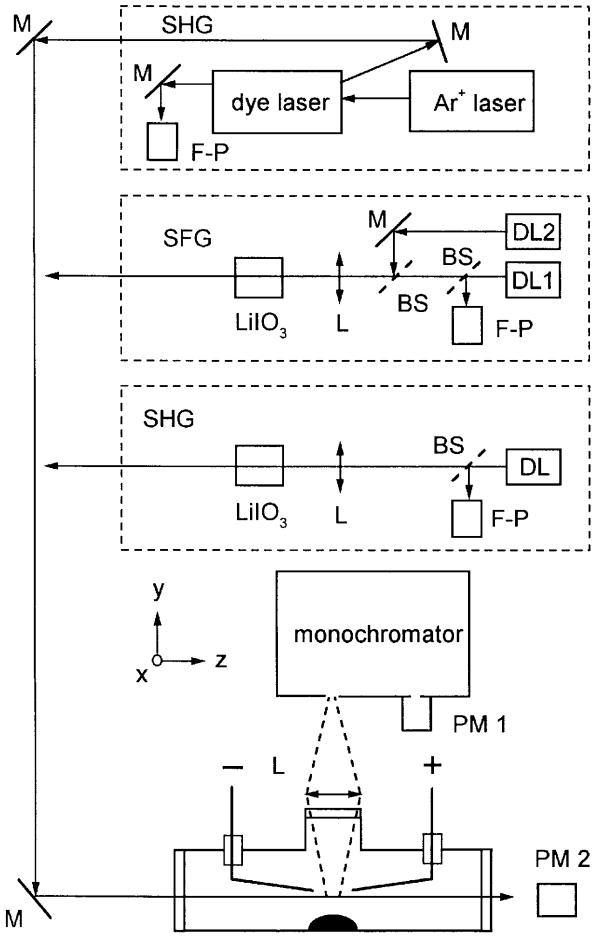

Fig. 2. Experimental arrangement: SHG: second harmonic generation; SFG: sum frequency generation; M: miror; F-P: Fabry-Perot interferometer; BS: beam splitter; DL: diode laser; L: lens; PM: photomultiplier.

2 Experiment

Figure 2 shows the experimental arrangement. The Pb vapour was generated in a T-shaped stainless-steel oven (inner diameter: 30 mm) with quartz windows at the ends. Ar or He were used as buffer gases. The central part of the oven, containing about 1 cm^3 high-purity Pb of natural isotope abundance, was heated resistively. The length of the Pb vapour column was about 40 mm. Metastable Pb atoms in the $6p^2\ ^3P_1$ and $6p^2\ ^3P_2$ states were produced in a DC discharge which was operated between two stainless-steel electrodes (diameter: 1 mm) in the Pb vapour-noble gas mixture. A small distance between the electrodes (8 mm) was necessary to prevent an unwanted, unstable electric discharge between the electrodes and the metal wall of the oven.

Narrow bandwidth lasers were used in the absorption measurements. The laser beams passed the generated Pb vapour column and the absorption was detected by a RCA 1P28 photomultiplier. The absorption signals were recorded by a digital oscilloscope and stored in a personal computer. To match the Pb resonance line at 283.39 nm, the radiation of a CW single-mode, frequency stabilized ring dye laser (Spectra Physics 380D; dye: mixture of Rh 6G and Rh 110) was intracavity frequency doubled in a KDP crystal. The power of the UV laser beam (diameter: 3 mm) inside the oven was about 20 μW. The scanning of the fundamental beam was controlled by a Fabry-Perot interferometer with free spectral range (f.s.r) of 2 GHz.

The laser radiation at the wavelengths 364.06 nm and 368.45 nm was obtained by sum frequency generation (SFG) using two single-mode CW laser diodes. A detailed description of this part of our experimental arrangement can be found in [5]. The radiation for the 364.09 nm line was generated by a Philips CQL 806 laser diode (DL1, power: 30 mW) and a Mitsubishi ML 60114 laser diode (DL2, power 50 mW). The lasers DL1 and DL2 were tuned to the wavelengths $\lambda_1 = 678.09$ nm and $\lambda_2 = 786.26$ nm, respectively. To obtain radiation at the 368.45 nm line the Mitsubishi laser diode was replaced by a Sharp LTO 16MDO laser diode (power: 30 mW) tuned to 806.88 nm. The beams of the DL1 and DL2, having the same polarisation, were spatially overlapped by the use of a mirror and a beam splitter. The overlapped beams were focused by a lens ($f = 100$ mm) into a $LiIO_3$ crystal. The crystal was 6 mm long and cut for type I SFG at 680 nm and 790 nm ($\Theta = 47°$). Behind the absorption oven the SFG radiation (incident power: about 15 nW) was separated from the two fundamental waves by a UV filter and detected by the photomultiplier. The continuous scanning (scan range: about 60 GHz) of the SFG radiation across the 364.06 nm as well as the 368.45 nm line was performed by scanning DL1. The beam of DL1 was splitted into two parts. The major part was used for SFG while the second, weaker part was used to obtain the frequency marks by a Fabry-Perot interferometer with 2 GHz f.s.r.

For the measurements of the 405.90 nm line the wavelength of an infrared single-mode laser diode (Sharp LTO 16MDO, power: 30 mW) was tuned by temperature to 811.80 nm. The required wavelength was obtained by extracavity second harmonic generation (SHG) in a $LiIO_3$ crystal. The intensity of the blue SHG laser light (power: 20 nW) was again detected by a photomultiplier. The fundamental radiation and the emission from the discharge were blocked by a 405 nm bandpass filter. A part of the fundamental beam was coupled out to set frequency marks with a Fabry-Perot interferometer while scanning across the line.

Typical spectra showing the laser absorption at the wavelengths of interest are given in Figure 3, together with the calculated relative intensities and the frequency positions of the isotope and hyperfine components. The data for the hyperfine constants and isotope shifts were taken from [6].

The centre of the oven with the lead sample was heated up to temperatures at which the peak absorptions of the investigated lines were about 50%. In the experiment on the resonance 283.39 nm line, the measurements of the integrated absorption yielded a Pb atom number density of about 4×10^{10} cm^{-3}, which corresponded to an oven temperature of 740 K [7]. In the experiments on the other

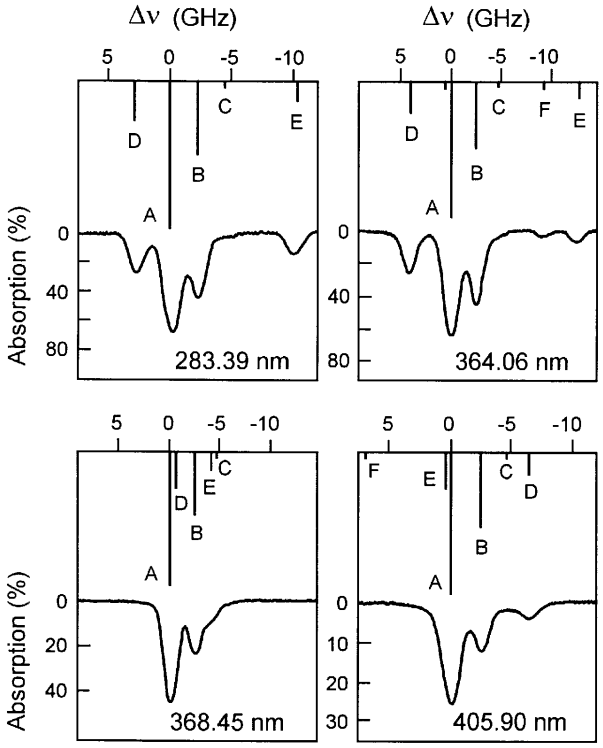

Fig. 3. Profiles of the Pb lines. The spectra were recorded at 10 mbar (283.3 nm line), 30 mbar (364.06 and 368.45 nm lines) and 50 mbar Ar pressure (405.90 nm line). The calculated relative intensities of the isotope and hyperfine components as well as their positions are given in the upper part of each spectrum. For all lines the transitions in ^{208}Pb, ^{206}Pb and ^{204}Pb are labeled with A, B, C, respectively, whereas the hyperfine structure components of ^{207}Pb are marked by D and E ($F = 1/2 \rightarrow F = 3/2$ and $F = 3/2 \rightarrow F = 3/2$, respectively) for the 283.39 nm line, by D, E, F, G ($F = 3/2 \rightarrow F = 3/2$, $F = 1/2 \rightarrow F = 1/2$, $F = 3/2 \rightarrow F = 1/2$ and $F = 1/2 \rightarrow F = 3/2$) for the 364.06 nm line, by D and E ($F = 3/2 \rightarrow F = 1/2$, and $F = 1/2 \rightarrow F = 1/2$) for the 368.45 nm line, and by D, E and F ($F = 3/2 \rightarrow F = 1/2$, $F = 5/2 \rightarrow F = 3/2$ and $F = 3/2 \rightarrow F = 3/2$) for the 405.90 nm line.

lines, the temperature was determined from the Doppler line widths (see the following section). The investigations on the 364.06 and 368.45 nm line were made at $T = 850$ K while the 405.90 nm line was studied at $T = 900$ K. The corresponding lead number densities were about 2×10^{12} cm^{-3} and 1×10^{13} cm^{-3}, respectively [7].

Under these conditions, very stable discharges (current: 30 mA) were obtained even at relatively high noble gas pressures, *i.e.*, 250 mbar and 800 mbar in Ar and He, respectively. At noble gas pressures bellow 20 mbar the discharge was unstable due to the influence of the metal walls of the oven.

The production and the annihilation of metastable atoms in a discharge are very complex processes. In general, the metastable atoms are mainly produced by dielectronic recombination of ions and collisional and radiative relaxation of the excited atoms. On the other hand, the annihilation of the metastables occurs due to collisions with electrons, ions and atoms either *via* back transfer to the higher atomic states and the continuum or directly to the ground state. Additional effects are expected to occur in the electrode regions.

To obtain the information about the spatial characteristics of the plasma, the discharge region was investigated spectroscopically by side-on line emission measurements. The discharge was imaged in 1:1 ratio onto the entrance monochromator slit of a 0.5 m Jarell-Ash monochromator (see Fig. 2). The spectra of the discharge showed strong lead emission lines emerging from the $7s\ ^3\mathrm{P}^o_J$ level but only very weak noble gas lines. This is a proof that the discharge is sustained in the Pb vapour. The noble gas atoms act mainly as collision partners for the Pb atoms. The spatial distribution of the excited short lived Pb atoms, which reflects the size of the discharge, was measured *via* intensities of the optically thin Pb lines by moving the imaging lens in the x and z directions (see Fig. 2). Assuming axial symmetry of the discharge and applying the Abel inversion method, we obtained the spatial distributions $N^*(r, z)$ of the excited atoms at different noble gas pressures (r: distance from the discharge axis). For buffer gas pressures between 30 mbar and 150 mbar, the discharge was found to be confined in a narrow cylindrical zone (diameter: 2 mm) between the electrodes. The radial distributions of the highly-excited Pb atoms in Ar and He are practically identical and independent on the noble gas pressure in the range between 30 and 150 mbar. Taking into account the thermal velocity of the electrons as the electron drift velocity and the mentioned dimension of the discharge zone, the estimated upper value of the electron number density was about 10^{11} cm^{-3} at a discharge current of 30 mA.

In addition, the distributions of the atoms in the $6p^2\ ^3\mathrm{P}_1$ and $6p^2\ ^3\mathrm{P}_2$ metastable states were investigated by absorption measurements at 368.45 nm and 405.90 nm, respectively. For this purpose, strongly collimated laser probe beams were shifted stepwise and parallel to the discharge axis. In this way we obtained the averaged optical depths $\overline{K_{\mathrm{met}}(r)}$ which are proportional to the averaged values $\overline{N_{\mathrm{met}}(r)L_z} = \int N_{\mathrm{met}}(r, z)\mathrm{d}z$. Here, N_{met} labels the number density of the metastable atoms and L_z is the length of the absorbing medium. The present experimental arrangement does not allow us to measure the axial dependence of the metastable number densities. At typical experimental conditions, the peak absorption depth at 368.45 nm in the region close to the discharge axis was 0.4. This absorption value and the estimated length (1 cm) of the discharge column with metastables yielded the value of 1×10^{12} cm^{-3} for the number density of the lead atoms being in the $6p^2\ ^3\mathrm{P}_1$ metastable state in the discharge axis. Note, that the measured portion of the lead atoms transferred to the lowest-lying metastable level in the region close to the centre of the discharge region is 50% of the ground state number density (see text above). Under the same experimental conditions, the number density of the lead atoms excited to the higher metastable $6p^2\ ^3\mathrm{P}_2$ state in the region close to the axis of

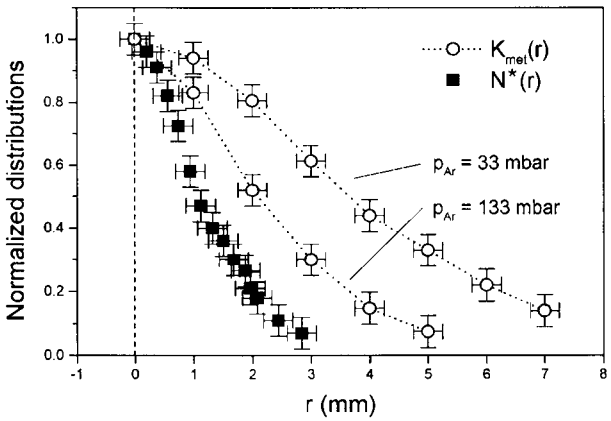

Fig. 4. Illustration of the diffusion of the metastable Pb atoms out of the discharge zone. $K_{\rm met}(r)$ is related to the spatial distributions of the metastable atoms for different pressures of argon. $N^*(r)$ shows the distribution of short-lived, highly-excited lead atoms in the discharge region for buffer gas pressures in the range between 30 mbar and 150 mbar. See text for further explanations.

the discharge was about 1.5×10^{10} cm^{-3}. The ratio of the measured metastable number densities agrees very well with the equilibrium value calculated for the experimental temperature $T = 850$ K. This ratio was found to be the same in the whole observed volume and in the total range of buffer gas pressures applied, *i.e.* the distributions of the lead atoms in the $6p^2\ ^3\mathrm{P}_1$ and $6p^2\ ^3\mathrm{P}_2$ states were identical. This fact indicates that the metastable states were strongly mixed due to collisions with noble gas atoms.

Figure 4 shows the distribution of highly excited, short-lived Pb atoms $N^*(r)$ in comparison with the distributions of the metastable Pb atoms at two different Ar pressures. The distributions of the metastables are represented by $K_{\rm met}(r)$. All distributions, normalized to unity for $r = 0$, were averaged over the z-axis. As one can see, the distributions of the metastables are significantly wider than the size of the discharge zone given by the distribution of the short-lived atoms. Variations of the noble gas density produced different spatial distributions of the metastable atoms, while the relative distribution of the atoms in short-lived excited states was not affected within the limits of experimental uncertainty. Qualitatively the same behaviour was observed for He. The size of the discharge zone was also independent of the buffer gas pressure but the diffusion of the metastable atoms from the discharge into the surrounding gas was much stronger in He than in Ar at the same pressures. This behaviour is very similar to the one recently seen for barium metastable atoms in buffer gas [8]. In the experiment on barium the effective lifetimes of the metastable atoms were determined by the comparison of the experimental and the theoretical diffusion distributions. For example, a rough evaluation of the present results yielded that the effective lifetime of the $6p^2\ ^3\mathrm{P}_2$ atoms is slightly shorter than 1 ms in Ar atmosphere at about 50 mbar.

It should be pointed out that the discharge zone becomes broader and changes its shape at buffer gas pressures above 150 mbar. This is mainly due to the extensive heating of the cathode and the expansion of the surrounding corona. However, even at these high pressures the distributions of the metastable atoms are wider than the distributions of the highly-excited, short-lived atoms. Due to the strong diffusion of the metastable atoms, it was possible to measure the profiles of the Pb lines outside the discharge without the influence of the plasma.

3 Measurements and results

The absorption coefficients of the considered lines were measured by continuous laser scanning across the lines (scan range: about 50 GHz). The laser line widths were at least two orders of magnitude smaller than the actual line profiles. The transmitted to incident laser light intensity ratio $I(\nu)/I_0(\nu)$ yields the absorption depth $k(\nu)L = -\ln[I(\nu)/I_0(\nu)]$, where $k(\nu)$ is the frequency dependent linear absorption coefficient and L is the effective length of the absorbing vapour column. The lines were measured in the impact region, where, as predicted by the Lindholm theory [9], the homogeneous profile of the single line can be analytically described by a Lorentz function. The normalized Lorentzian line profile can be written as:

$$P_{\rm L}(\nu) = \frac{1}{2\pi} \frac{\Gamma_{\rm b}}{(\nu_0 - \nu + \Gamma_{\rm s})^2 + (\Gamma_{\rm b}/2)^2} \cdot \tag{1}$$

Here, $\Gamma_{\rm b}$ and $\Gamma_{\rm s}$ are the line broadening and shift rates, respectively, expressed in frequency units (s^{-1}). The $\Gamma_{\rm b}$ is the line full width at half maximum (FWHM), henceforth referred to as half-width. The quantities $\Gamma_{\rm b}$ and $\Gamma_{\rm s}$ can be written as:

$$\Gamma_{\rm b} = \Gamma_{\rm nat} + \Gamma^A_{\rm coll} = \Gamma_{\rm nat} + \gamma_{\rm b} N_A, \tag{2}$$

and

$$\Gamma_{\rm s} = \gamma_{\rm s} N_A. \tag{3}$$

Here, $\Gamma_{\rm nat}$ is the natural broadening rate, $\gamma_{\rm b}$ and $\gamma_{\rm s}$ are the collisional broadening and shift rate coefficients due to the particular perturber and N_A is the number density of the perturber.

The profiles $k(\nu)$ of the measured lead lines are compositions of several hyperfine and isotope components. The profiles of the particular components are generally of the Voigt type, *i.e.* the convolution of a Gaussian (Doppler broadening) and Lorentzian function (natural and collisional broadening). The normalized Voigt profile is usually [10] represented in the form:

$$P(\nu) = \frac{1}{\Delta\nu_{\rm D}\sqrt{\pi}} H(\nu_0 - \nu, \alpha), \tag{4}$$

where $H(\nu_0 - \nu, \alpha)$ is the Voigt function for detuning $(\nu_0 - \nu)$ from the line centre ν_0, with parameter α defined as:

$$\alpha = \Gamma_{\rm b}/2\Delta\nu_{\rm D}, \tag{5}$$

with the Doppler width $\Delta\nu_\mathrm{D}$ which is given by:

$$\Delta\nu_\mathrm{D} = (\nu_0/c)(2kT/M)^{1/2}. \quad (6)$$

Here, c is the velocity of light, k is the Boltzmann constant and M is the mass of the optically active atoms.

3.1 Measurement of the broadening rate coefficients

Using the known structures of the measured lines we calculated the theoretical line profiles for different parameters α as composition of several Voigt functions. The calculated profiles were normalized to be equal to unity for the central frequency of the strongest components (transitions in the isotope ^{208}Pb). The experimental profiles $k(\nu)$, measured at various noble gas pressures were normalized in the same manner as the theoretical profiles. Fitting the experimental profiles into the field of the theoretical line shapes yields the values α for the particular noble gas pressures. With known experimental temperatures, *i.e.* known Doppler widths, the Lorentzian half-widths Γ_b of the lines were obtained as functions of the number density of the perturber gas. From this data one obtains the values for the corresponding broadening rate coefficients γ_b.

As mentioned in the previous section, the measurements at 283.39 nm were performed at lead number density of 4×10^{10} cm^{-3}. The atomic density was evaluated from the measured absorption depth of the optically thin resonance line using the estimated value for the effective length of the lead vapour column (40 mm). The corresponding temperature (740 K), determined from the lead vapour pressure curve given in [7], yielded the value of 860 MHz for the Doppler constant of the 283.39 nm line. In the case of the lines related to the metastable states, the experimental temperature and the corresponding lead number density were higher. Under these conditions the resonance line was optically thick. Therefore, we applied a different method to obtain the experimental temperature. We measured the line widths of the strongest components of the 368.45 nm and 405.90 nm lines, in a wide range of He pressures above 30 mbar. The extrapolation of the measured line widths to zero noble gas pressure yielded the corresponding Doppler FWHM. For instance, this procedure gave a Doppler FWHM of 1100 MHz for the Pb 405.90 nm line, which yielded a Doppler constant of $\Delta\nu_\mathrm{D} = 660$ MHz, *i.e.* a temperature $T = 900$ K. In the same way, we obtained the temperature $T = 850$ K for the experimental conditions in which the lines Pb 364.06 and Pb 368.45 nm were measured.

The values for the Lorentzian half-widths Γ_b measured in Ar and plotted *versus* argon number density N_Ar are given in Figure 5. A similar behaviour (not shown here) was obtained with He as a buffer gas. The linear dependence of Γ_b on the perturber number density demonstrates that the measured half-widths are essentially due to collisions with noble gas atoms. The natural broadening rates for the considered lines are of the order of magnitude of 10^7 s^{-1}, and thus, negligible in comparison with the broadening rates. The evaluated collisional-broadening rate coefficients γ_b for all lines and both buffer gases are given in Table 1. The broadening rate coefficients of the 283.39 nm line by He and Ar, as published in [4], are also listed in Table 1.

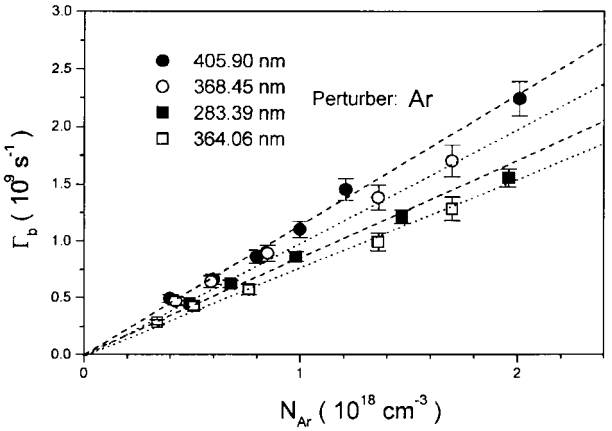

Fig. 5. Collisional-broadening rates Γ_b of the Pb lines in dependence on argon number density N_Ar measured at 740 K (283.39 nm), 850 K (364.06 and 368.45 nm) and 900 K (405.90 nm). The dashed straight lines are least squares fits to the data points.

Table 1. Broadering and shift rate coefficient of the 283.39 nm, 364.06 nm, 368.45 nm and 405.90 nm lines of Pb due to collisions with Ar and He perturbers. The uncertainties given are statistical uncertainties (*a*: data from Ref. [4]).

Line (nm)	Perturber	γ_b (10^{-10} cm^3 s^{-1})	γ_s (10^{-10} cm^3 s^{-1})
283.39	Ar	8.5 ± 0.5	-2.7 ± 0.3
		$(7.4 \pm 0.2)^a$	$(-2.6 \pm 0.1)^a$
	He	9.7 ± 0.5	$+1.3 \pm 0.2$
		$(10.2 \pm 1)^a$	$(+0.9 \pm 0.3)^a$
364.06	Ar	7.8 ± 0.5	-3.5 ± 0.5
	He	9.3 ± 0.5	$+0.5 \pm 0.3$
368.45	Ar	9.6 ± 0.5	-3.0 ± 0.5
	He	10.5 ± 0.5	$+0.5 \pm 0.2$
405.90	Ar	11.4 ± 0.5	-2.8 ± 0.3
	He	12.4 ± 0.5	$+0.26 \pm 0.1$

3.2 Measurements of the shift rate coefficients

The collisional shifts of the 283.39 nm and 405.90 nm lines were also determined in dependence on the buffer gas pressure. In the case of the resonance line, the collisional shift Γ_s was measured by comparing the line positions of the strongest non- blended component at high noble gas pressures with that at very low pressure (0.1 mbar).

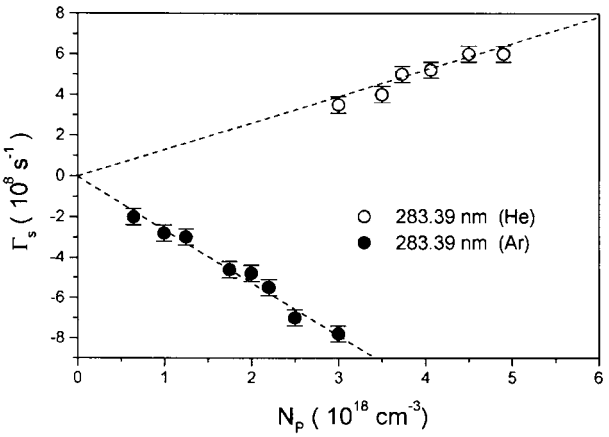

Fig. 6. Plot of the collisional-shift rates Γ_s of the Pb 283.39 nm line in dependence on the perturber density N_P measured at 740 K in Ar and He. The dashed straight lines are least squares fits to the data points.

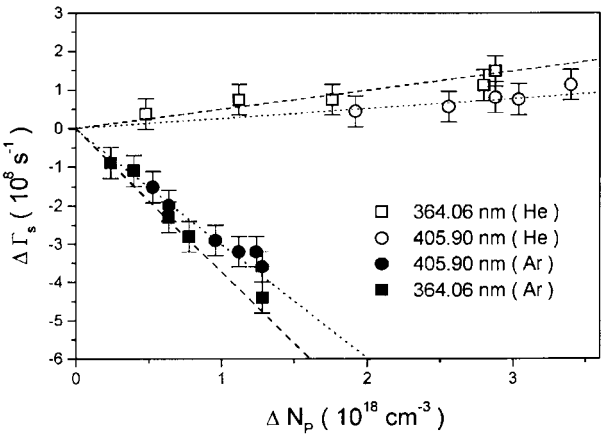

Fig. 7. Plot of the collisional-shift rate difference $\Delta\Gamma_s$ of the 364.06 and 405.90 nm lines in dependence on the perturber density difference ΔN_P (see text for explanation). The lines 364.06 nm and 405.90 nm were measured at $T = 850$ K and $T = 900$ K, respectively, for both buffer gases (Ar, He). The dashed straight lines are least squares fits to the data points.

The dispersion was taken from the transmission peaks of the Fabry-Perot interferometer (f.s.r.: 2 GHz). The plot of the measured Γ_s for the resonance line in dependence on the noble gas densities is displayed in Figure 6.

The shifts of the 364.06, 368.45 and 405.90 nm lines, were determined by a comparison of the line positions at noble gas pressures of $p_0 = 30$ mbar with line positions at higher pressures (p). The lower pressure limit was determined by appearing instabilities of the discharge. The measured line shift differences $\Delta\Gamma_s$ in dependence on the buffer gas number density differences $\Delta N_A = N_A(p) - N_A(p_0)$ are plotted in Figure 7. For the sake of clearness, the data for the 368.45 nm line are not shown. They lie very close to the data for the 364.06 nm line.

As one can see in Figures 6 and 7, Ar gas causes a red shift for all investigated Pb lines, while He collisions produce relatively small blue shifts. The collisional shift rate coefficients derived from these data are listed in Table 1. The experimental errors of our broadening and shift rate coefficients in Table 1 are due to statistical uncertainties only. Additionally one has to take into account systematic errors of about 5% caused by uncertainties in the determination of the temperature and the noble gas pressure. Our broadening and shift rate coefficients for the Pb 283.39 nm line for Ar and He are in good agreement with the data published by Kötteritzsch *et al.* [4] (see Tab. 1) if our estimated systematic errors are also taken into account. The rate coefficients for the other Pb lines have been measured for the first time as mentioned above.

We did not try to extract the Pb-noble gas long range difference interaction potentials from the broadening data because we do not know yet whether the broadening is governed by van der Waals interaction. In principle, we could use model potential, such as the Lennard-Jones potential [2,3]. However, such analysis often does not give definite results or gives very crude data only. Theoretical calculations of the Pb-noble gas potentials are planned.

The authors gratefully acknowledge financial support by Ministry of Education, Science, Reseach and Technology (Federal Republic of Germany) and the Ministry of Science and Technology (Republic of Croatia).

References

1. S.Y. Ch'en, M. Takeo, Rev. Mod. Phys. **29**, 20 (1957).
2. N. Allard, J. Kielkopf, Rev. Mod. Phys. **54**, 1103 (1982).
3. J.R. Fuhr, A. Lesage, *Bibliography on Atomic Line Shapes and Shifts*, NIST Special Publication 366 (U.S. Government Printing Office, Washington D.C., 1994).
4. M. Kötteritzsch, W. Gries, A. Hese, J. Phys. B: At. Mol. Opt. Phys. **25**, 913 (1992).
5. J. Franzke, Spectrochim. Acta **B**, 1595 (1998).
6. W. Hüffer, Ph.D. thesis, Köln, 1982.
7. A.N. Nesmeyanov, *Vapor pressure of elements* (Academic Press, New York, 1963).
8. C. Vadla, K. Niemax, V. Horvatic, R. Beuc, Z. Phys. D **34**, 171 (1995).
9. E. Lindholm, Arkiv. Mat. Astr. Phys. A **32**, 17 (1945).
10. D.W. Posener, Austr. J. Phys. **12**, 184 (1959).